STUDIES IN RAPIDITY AND p_T-SPECTRA OF PIONS IN HIGH ENERGY NN, NA AND AA COLLISIONS: A COMPREHENSIVE APPROACH

BHASKAR DE* and S. BHATTACHARYYA†

Physics and Applied Mathematics Unit (PAMU),
Indian Statistical Institute, Kolkata-700108, India
**bhaskar_r@www.isical.ac.in*
†bsubrata@www.isical.ac.in

P. GUPTAROY‡

Department of Theoretical Physics,
Indian Association for the Cultivation of Sciences,
Kolkata-700032, India

Received 14 April 2002

The present paper aims at testing a very simple approach to interpret the characteristics of inclusive production of pions in high energy NA and AA collisions by a somewhat in-depth analysis of the same for NN interactions; and also at reporting here thus some interesting observations made on the nature of rapidity and transverse momentum spectra of the produced pions. And this approach is built upon a newly offered master formula holding the key for converting the results of high energy nucleon–nucleon (NN) collision to the corresponding observables on differential and inclusive cross-sections for both nucleon–nucleus and nucleus–nucleus (heavy ion) collisions in a generalized form. The proposed formulae, used in a somewhat phenomenological way, can provide modestly reliable parametrization of data in the broad range of collision energy and the varied range of projectile-target combinations. This opens up the possibility of understanding in a quite unified manner the large amount of data on the rapidity and transverse momentum spectra in a wide range of interactions and energies starting right from ISR, rather Bevelac, to the relativistic heavy ion collisions (RHIC) via the various collider scales of energy. The agreements between the data and calculations, in most cases, are quite satisfactory both qualitatively and quantitatively. While highlighting this success, the limitation of the approach has also been pointed out in the end as clearly and categorically as possible.

Keywords: Inclusive cross-section; heavy ion collision.

PACS numbers: 13.60.Hb, 25.75.-q

‡On leave from Department of Physics, Raghunathpur College, P.O.: Raghunathpur 723133, Dist.: Purulia (WB), India.

1. Introduction

The importance of studying the rapidity and transverse momentum spectra of the pion secondaries in high energy particle–particle, particle–nucleus or nucleus–nucleus collisions is quite well known. Pions constitute the most significant bulk of the produced secondaries for which they call for special attention. Quite admittedly, the present work pertains to some old issues of the rapidity (pseudorapidity) and transverse momentum spectra of only the pions produced in high energy nucleon–nucleon (NN), nucleon–nucleus (NA), and finally in nucleus–nucleus (AA) collisions at CERN or at relativistic heavy ion collider (RHIC) at BNL-USA. Our objective here is to provide a unified, useful and simple approach to link up the results of high energy nucleon–nucleon collision to the results of the corresponding observables for a set of nucleon–nucleus and nucleus–nucleus collisions. In fact, this study made in some detail on the rapidity and transverse momentum spectra is an offshoot of some of our previous work on average phase space density of pionisation.[1,2] What we try to build up here, somewhat exhaustively, is essentially a different way of looking at old issues by imparting overwhelming experimental support and some hints as well on its possible valuable import to what was earlier initiated by Peitzmann[3] in a tentative and somewhat casual manner. It is to be noted that the present study is made here exclusively on pions in a charge-independent manner.

The organization of the paper is as follows. In Sec. 2 we give a brief outline of Peitzmann's approach. In Sec. 3 we present the results obtained by applying this approach to the analysis of rapidity spectra for pion production in nucleon–nucleus (NA) and nucleus–nucleus (AA) collisions. In Sec. 4 we apply the Peitzmann approach in analyzing the transverse momentum spectra for pions in an array of a large number of proton–nucleus and nucleus–nucleus collisions in the heavy ion colliders. The last section (Sec. 5) is devoted to summarizing our conclusions and emphasizing the points of interest.

Once again, let us state our position here. What we would stress upon is that we attempt to broaden here the parametrization of massive data by the proposed and some already existing formulae which were applied so far randomly and/or in a very stray manner for one, two or a very few selected collisions. The real worth and merit of any relationship or approach cannot be explored by analyzing discretely one or two cases in isolation or in a haphazard manner; but that can be appreciated only by extensive and intensive analysis of a large band of reactions with mass-numbers ranging from $A = 2$ (for Deuteron) to $A = 238$ (for Uranium), including especially the case of $A = 207$ (for Lead), over a wide energy range in a cohesive and consistent way.

2. Transition from NN → NA and NN → AA Collisions: The Empirical Route

Following Peitzmann[3] and also the work of Schmidt and Schukraft[4] we propose here a generalized empirical relationship between the inclusive cross-section for pion

production in nucleon–nucleon collision and the same for nucleus–nucleus collisions as given below:

$$E\frac{d^3\sigma}{dp^3}(\mathrm{AB})^{\pi^0 X} = (\mathrm{A}\cdot\mathrm{B})^{\epsilon(y,p_T)} E\frac{d^3\sigma}{dp^3}(\mathrm{PP})^{\pi^0 X}\,, \tag{1}$$

where $\epsilon(y, p_T)$ could be expressed in the factorization form $\epsilon(y, p_T) = f(y)g(p_T)$. While investigating a specific nature of dependence of the two variables (y and p_T), either of them is assumed to remain constant. Speaking in clearer terms, if and when rapidity dependence is studied by the experimental groups the transverse momentum is treated to be constant and the vice-versa. So the effective formulae turn into

$$E\frac{d^3\sigma}{dp^3}(\mathrm{AB})^{\pi^0 X} \sim (\mathrm{AB})^{f(y)} E\frac{d^3\sigma}{dp^3}(\mathrm{PP})^{\pi^0 X}\,, \tag{2}$$

$$E\frac{d^3\sigma}{dp^3}(\mathrm{AB})^{\pi^0 X} \sim (\mathrm{AB})^{g(p_T)} E\frac{d^3\sigma}{dp^3}(\mathrm{PP})^{\pi^0 X}\,. \tag{3}$$

The main bulk of work, thus, converges to the making of an appropriate choices of forms for $f(y)$ and $g(p_T)$ separately. And the necessary choices are to be made on the basis of certain premises and physical considerations which do not violate the canons of high energy interactions.

3. Rapidity (Pseudorapidity) Distributions of Pions

3.1. PP *collisions*

ow for b Applying the concept of both limiting fragmentation and the Feynman scaling hypothesis we attempt at providing first a fit to the data on pseudorapidity distributions measured by Thome' *et al.*[5] for proton–proton collisions at several $\sqrt{s}$ values, ranging from $\sqrt{s} = 23.6$ GeV to 62.8 GeV with a parametrization by the three-parameter formula:

$$\frac{1}{\sigma}\frac{d\sigma}{dy} = C\left(1 + \exp\frac{y - y_0}{\triangle}\right)^{-1}. \tag{4}$$

The choice of the above form made by Thome' *et al.*[5] was intended to describe conveniently the central plateau and the fall-off in the fragmentation region by means of the parameters y_0 and $\triangle$ respectively. For all five energies in PP collisions the value of $\triangle$ was chosen to be ~ 0.55. And this value of $\triangle$ is assumed to remain the same though, even for $\mathrm{P\bar{P}}$ collision.

3.2. $\mathrm{P\bar{P}}$ *collisions*

The data sets were obtained from the results of UA(5) Collaboration[6] upto $\sqrt{s} =$ 540 GeV. But the CDF data at $\sqrt{s} = 900$ GeV and 1.8 TeV were collected from F. Demarteau *et al.*[7]

3.3. *Common procedural steps*

Now for both PP and P$\bar{\text{P}}$ reactions at various energies the fits for the rapidity (pseudorapidity) spectra are phenomenologically obtained by us through the making of suitable choices of C and y_0 which would be given in tabular forms in Tables 1(a) and 1(b). The fits at various energies with the assumption of equivalence between PP and P$\bar{\text{P}}$ reactions at high energies are shown in the adjoining diagrams (Figs. 1 and 2).

(*i*) PP *Collision*:

Table 1a. Parameter values for PP collisions at various accelerator energies.

$\sqrt{s}_{\text{NN}}$ (GeV)	C	y_0	$\frac{\chi^2}{ndf}$
23.6	1.516 ± 0.022	2.871 ± 0.049	1.309
30.8	1.766 ± 0.021	2.791 ± 0.024	0.390
45.2	1.862 ± 0.022	3.139 ± 0.039	0.653
53.2	2.004 ± 0.024	3.077 ± 0.033	0.926
62.8	2.096 ± 0.029	3.187 ± 0.040	1.270

(*ii*) P$\bar{\text{P}}$ *Collision*:

Table 1b. Values of the parameters: P$\bar{\text{P}}$ colliders at various energies.

$\sqrt{s}_{\text{NN}}$ (GeV)	C	y_0	$\frac{\chi^2}{ndf}$
53	2.01 ± 0.03	2.70 ± 0.04	1.67
540	3.19 ± 0.01	3.86 ± 0.04	1.50
900	3.85 ± 0.02	3.89 ± 0.05	1.54
1800	4.453 ± 0.044	5.283 ± 1.173	0.434

3.4. *Nucleus–nucleus collisions and the nature of fits*

The fits to the data on $\frac{dn}{d\eta}$ versus η (or y) for PP and P$\bar{\text{P}}$ are given in Figs. 1 and 2 respectively. In order to study the nature of dependence of both C and y_0 on $\sqrt{s}$ we propose here in empirical manner two expressions in the following forms as represented by Fig. 3:

$$C = 0.65 \ln \sqrt{s_{\text{NN}}} - 0.59\,, \tag{5}$$

$$y_0 = 0.55 \ln \sqrt{s_{\text{NN}}} + 0.88\,. \tag{6}$$

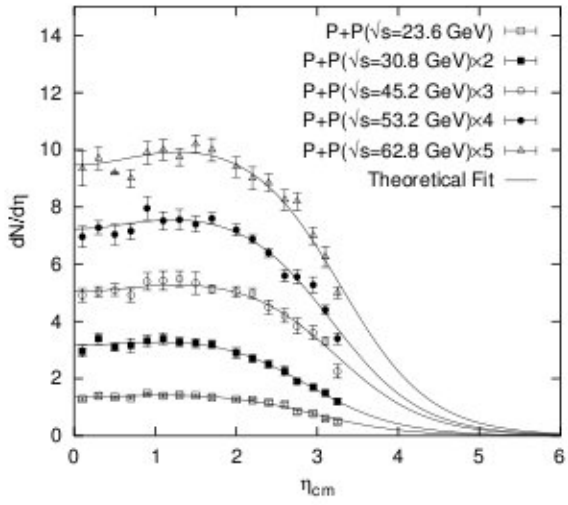

Fig. 1. Rapidity spectra for secondary pions in PP collisions at various c.m. energies. The various experimental points are from Ref. 5. The solid curves depict the theoretical fits based on Eq. (4).

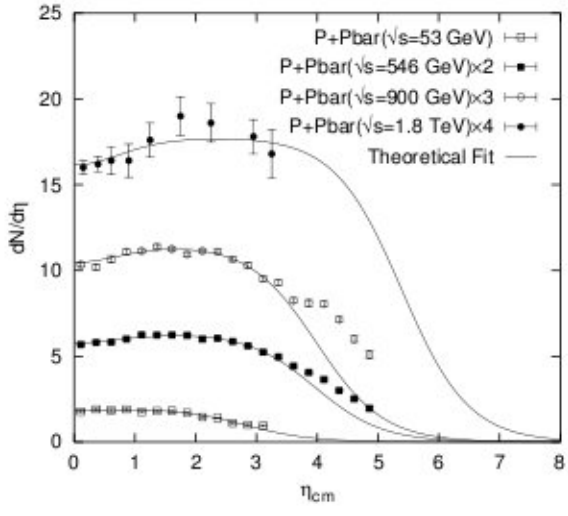

Fig. 2. Plot of $\frac{dN}{d\eta}$ versus $\eta_{\rm cm}$ for secondary pions in $P\bar{P}$ collisions at different energies. The various experimental data-points are taken from Refs. 6 and 7. The solid curvilinear lines represent the theoretical fits on the basis of Eq. (4).

It is to be noted that we do not consciously call the expressions (5) and (6) "fit"(s), as we cannot and do not get here χ^2/ndf values for C versus $\sqrt{s}_{\rm NN}$ and y_0 versus $\sqrt{s}_{\rm NN}$ relations quite favorably, because $\sqrt{s}_{\rm NN}$ values are extremely widely distributed with a range from $\sqrt{s}_{\rm NN}$ (GeV) = 53 GeV to $\sqrt{s}$ = 1800 GeV for $P\bar{P}$ collisions and there are in total only two intermediate posts for $P\bar{P}$ reactions at $\sqrt{s}_{\rm NN}$ (GeV) = 540 GeV and $\sqrt{s}_{\rm NN}$ (GeV) = 900 GeV. But, for PP interactions the data points are for relatively much closer energies yielding better results. Still,

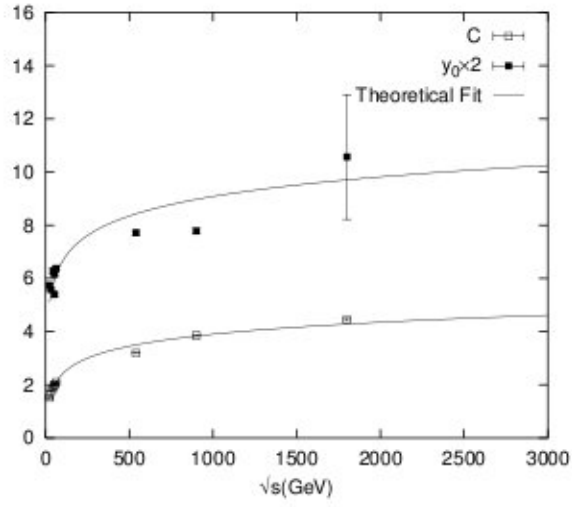

Fig. 3. Values of C and y_0 as a function of c.m energy, $\sqrt{s}$. The data-type points (closed and open squares) are from Tables 1(a) and 1(b). The solid curves are drawn on the basis of Eqs. (5) and (6).

even in the case of PP collision, the range is too small from $\sqrt{s_{\rm NN}} = 23$ GeV to $\sqrt{s_{\rm NN}} = 62.8$ GeV. However, this is done here just for gaining insights in their nature and for purposes of extrapolation to the energies [in the frame of $\sqrt{s_{\rm NN}}$] for various nucleon–nucleus and nucleus–nucleus collisions. The specific energy [in the c.m. system, $\sqrt{s_{\rm NN}}$] for every nucleon–nucleus or nucleus–nucleus collision is first worked out by converting the laboratory energy value(s) in the required c.m. frame energy value(s). Thereafter the values of C and y_0 to be used for computations of inclusive cross-sections of nucleon–nucleon collisions at particular energies of interactions are extracted from the plots Figs. 1 and 2 at the corresponding energy.

Our next step is to explore the nature of $f(y)$ which is envisaged to be given generally by a polynomial form given below:

$$f(y) = \alpha + \beta y + \gamma y^2 , \tag{7}$$

where α, β and γ are the coefficients to be chosen separately for each AB collisions (and also for AA collisions when the projectile and the target are the same). Before dealing with this issue in detail, let us make a point here. The suggested choice of form in expression (7) is not altogether fortuitous. In fact, we got the clue from one of the previous work by one of the authors (SB)[8] here pertaining to the studies on the behavior of the EMC effect related to the lepto-nuclear collisions. In the recent past Hwa *et al.*[9] also made use of this sort of relationship in a somewhat different context. Now we go back to our original discussion. Combining Eqs. (2) and (7) the final working formula for $\frac{dN}{dy}$ in various AB (or AA) collisions can be expressed by the following relation:

$$\frac{dN}{dy}(\mathrm{AB})^{\pi^0 X} = (\mathrm{AB})^{\alpha+\beta y+\gamma y^2} \frac{dN}{dy}(\mathrm{PP})^{\pi^0 X} . \tag{8}$$

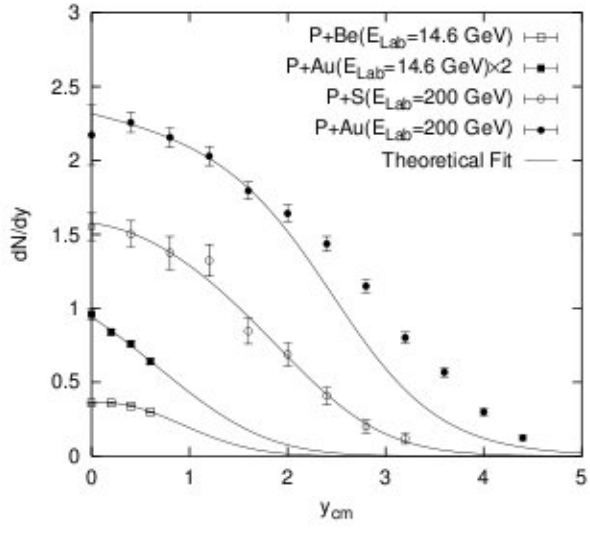

Fig. 4. Rapidity spectra for secondary pions produced in various proton–nucleus interactions at $E_{\mathrm{Lab}} = 14.6$ and 200 GeV. The different experimental points are from Ref. 18. The solid curves provide the theoretical fits on the basis of Eq. (8).

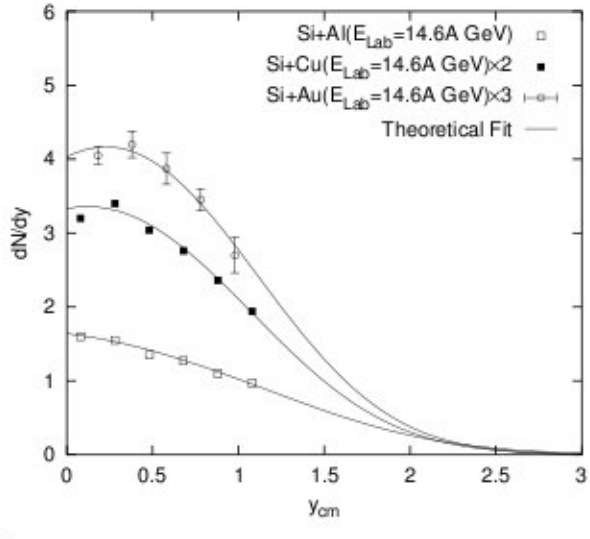

Fig. 5. Plot of $\frac{dN}{dy}$ versus y_{cm} for secondary pions produced in various silicon induced collisions at $E_{\mathrm{Lab}} = 14.6$ A GeV. The different experimental data-points are taken from Ref. 19. The solid curves represent the theoretical fits on the basis of Eq. (8).

The diagrams (Figs. 4–10) depict the nature of fits to the data on nucleus–nucleus collisions with regard to the rapidity (pseudorapidity) variable under consideration. Both the qualitative nature of data and its quantitative measures are well reproduced by the expression (8), though suitable normalizations for quantitative measures have been adopted whenever necessary.

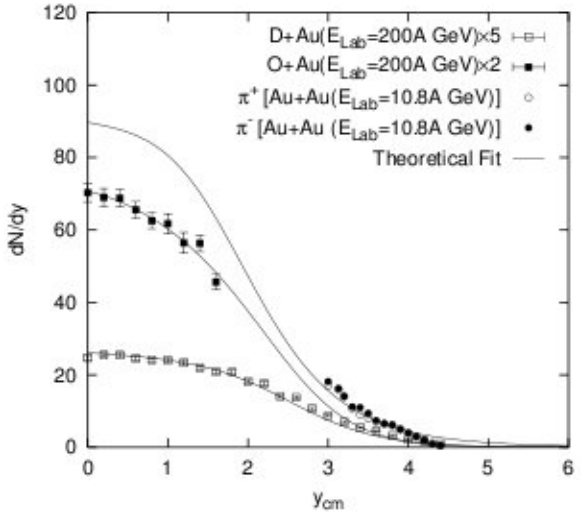

Fig. 6. Dependence of $\frac{dN}{dy}$ on $y_{\rm cm}$ for secondary pions produced in D–Au, O–Au and Au–Au collisions at $E_{\rm Lab} = 200$ A and 10.8 A GeV. The different experimental points are from Refs. 20 and 21. The solid curvilinear lines depict the theoretical fits on the basis of Eq. (8).

Some comments, specific to this work, are in order here: (i) the energy ranges for the fits to the data (and/or predictions for it) span from $\sqrt{s} = 23.6$ GeV to $\sqrt{s} = 1.8$ TeV for nucleon–nucleon collisions; and $E_{\rm Lab} = 10.8$ A GeV (Au + Au collisions) to $E_{\rm Lab} = 200$ A TeV (Ca–C collision) for nucleon–nucleus and nucleus–nucleus collisions. (ii) As there is a valid and acceptable relationship between $\frac{dn}{dy}$ and $\frac{dn}{d\eta}$ and between y and η, we have used any data whatever is available so far, irrespective of y and η. Besides, this work is done not on the basis of any approximation or assumption of near equality between rapidity and pseudorapidity. In fact, in all our calculations we have put the exact and existing relationship between the two.[10] (iii) Differences between PP and P$\bar{\rm P}$ reactions have, for all practical purposes, been neglected here, as the annihilation channels at high energies do not contribute significantly.[11] (iv) The plots of both $\sqrt{s}$ versus C values and $\sqrt{s}$ versus y_0 depict a near saturation at asymptotically high energies which could be visualized as the saturation plateau for pionization. (v) The physical nature on convexity–concavity of $\frac{dn}{d\eta}$ $\left(\text{or } \frac{dn}{dy}\right)$ veersus η (or y)[12] is nicely reproduced by the polynomial form considered here. (vi) In Table 2 we present in the last column the χ^2/ndf values for model-based results which show satisfactory agreement with data excepting the cases of Ca + C, Si + Ag (Figs. 8 and 9) and Au + Au collisions at 10.8 A GeV (Fig. 6). In the former two cases the data appear as bar graphs and as no discrete points, for which χ^2/ndf values are not at all satisfactory. But for Au + Au collisions at 10.8 A GeV (Fig. 6) data are obtained for an extremely small range of y-values; so the χ^2/ndf values do not give any favorable disposition.

Table 2. Fit parameters for rapidity spectra in nuclear collisions at different energies.

Collision	E (GeV)	α	β	γ	χ^2/ndf
P + Be	14.6	-0.114 ± 0.0008	0.103 ± 0.006	-0.312 ± 0.009	0.018
P + S	200	0.048 ± 0.010	-0.011 ± 0.007	-0.034 ± 0.007	0.615
P + Au	14.6	0.003 ± 0.001	-0.07 ± 0.01	-0.05 ± 0.03	0.402
P + Au	200	0.104 ± 0.003	-0.01 ± 0.003	0	0.226
D + Au	200 A	0.228 ± 0.001	-0.006 ± 0.001	0	1.427
O + Au	200 A	0.407 ± 0.002	-0.007 ± 0.002	-0.006 ± 0.001	0.558
Ca + C	2×10^5 A	0.467 ± 0.015	-0.013 ± 0.006	-0.002 ± 0.001	—
Si + Al	14.6 A	0.187 ± 0.001	-0.017 ± 0.008	-0.03 ± 0.01	0.052
Si + Cu	14.6 A	0.167 ± 0.001	0.027 ± 0.009	-0.07 ± 0.01	0.065
Si + Ag	5000 A	0.57 ± 0.006	-0.01 ± 0.004	-0.003 ± 0.002	—
Si + Au	14.6 A	0.119 ± 0.001	0.04 ± 0.01	-0.07 ± 0.02	0.518
S + S	200 A	0.45 ± 0.005	-0.033 ± 0.004	-0.008 ± 0.002	1.001
S + Ag	200 A	0.446 ± 0.001	-0.005 ± 0.001	-0.016 ± 0.001	1.529
S + Au	200 A	0.412 ± 0.018	-0.028 ± 0.0003	-0.018 ± 0.001	0.193
Au + Au	10.8 A	0.5	0.003	0.006	—
Au + Au (RHIC) 0–6% Centrality	8450 A	0.516 ± 0.001	-0.004 ± 0.001	0	0.036
Au + Au (RHIC) 45–55% Centrality	8450 A	0.336 ± 0.001	-0.003 ± 0.001	0	0.032
Pb + Pb	160 A	0.452 ± 0.001	-0.013 ± 0.001	-0.02 ± 0.0003	0.251

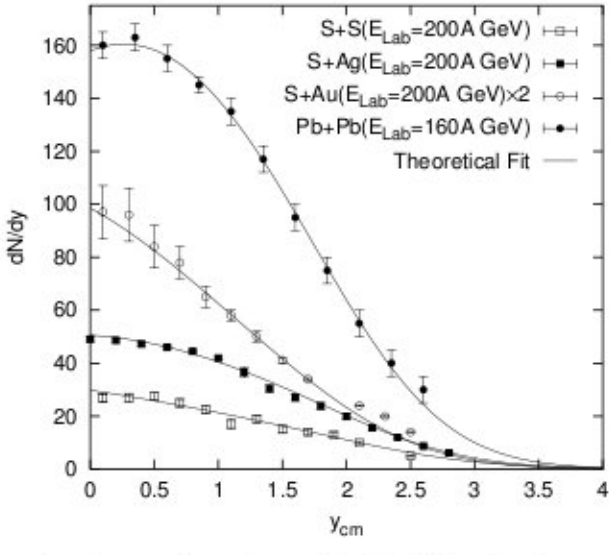

Fig. 7. Rapidity spectra for secondary pions produced in different nucleus–nucleus reactions at $E_{\mathrm{Lab}} = 160$ A and 200 A GeV. The various experimental data are taken from Refs. 18, 20 and 22. The solid curves represent the theoretical fits on the basis of Eq. (8).

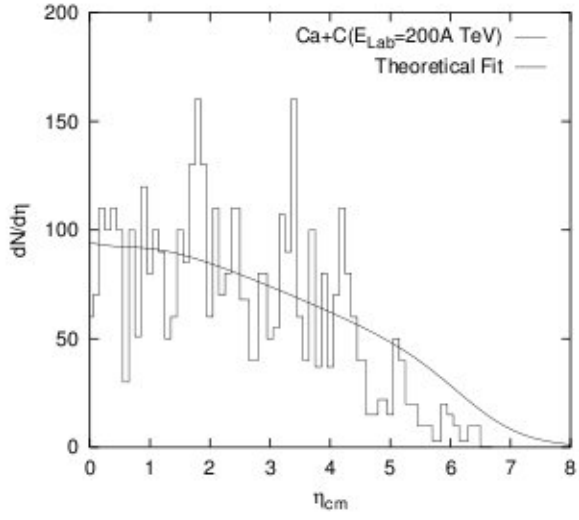

Fig. 8. Nature of dependence of $\frac{dN}{d\eta}$ on $\eta_{\rm cm}$ for secondary pions in Ca–C collisions at $E_{\rm Lab}$ = 200 A TeV. The experimental bar-graph is from Ref. 23. The solid curvilinear line is drawn on the basis of Eq. (8).

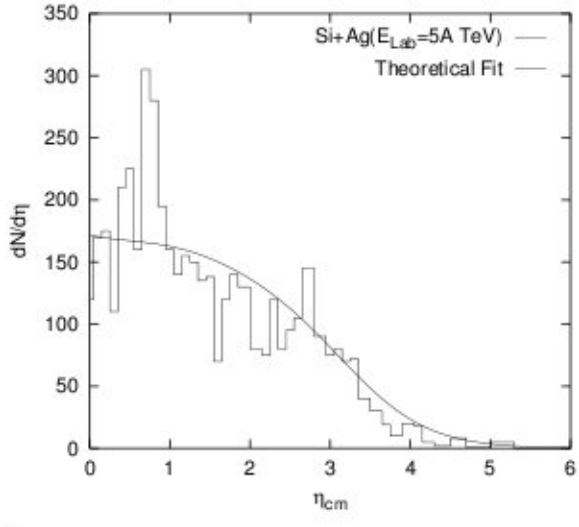

Fig. 9. Plot of $\frac{dN}{d\eta}$ versus η for secondary pions in Si–Ag collisions at $E_{\rm Lab}$ = 5 A TeV. The experimental bar graph is from Ref. 23. The solid curvilinear line is drawn on the basis of Eq. (8).

(vii) However, the natures of fits to the latest RHIC data (reference is in figure caption) on Au + Au collisions at $\sqrt{s_{\rm NN}} = 130$ GeV for minimum and for maximum centrality shown in the same figure (Fig. 10) are somewhat different; but the χ^2/ndf values for both of them are quite satisfactory. This provides a strong boost to try the model in analyzing further the various other oncoming experimental results from either the RHIC now in operation, or the forthcoming LHC at CERN.

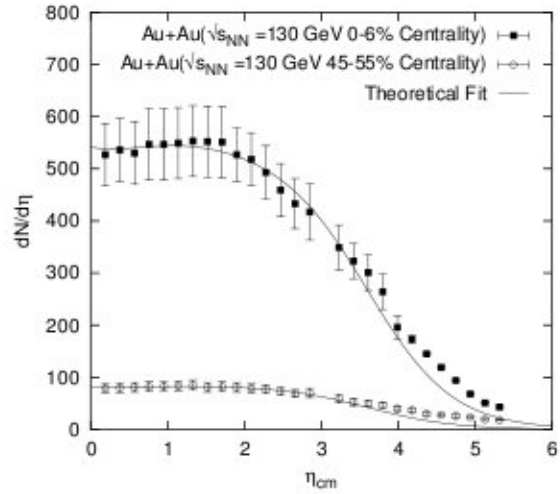

Fig. 10. Rapidity spectra for production of secondary pions in Au–Au collisions at $E_{\rm Lab}$ = 8.5 A TeV. The various experimental points are from RHIC.[24] The solid curves are drawn on the basis of Eq. (8).

4. Transverse Momentum Spectra of Pions in Nuclear and PP Collisions

This section comprises two subsections. In Subsec. 4.1 we give the outline of the basic physics of transverse momentum spectra in PP collisions and put forward in a concrete form the necessary working formulae for PP and the parameter values to be put into use. In Subsec. 4.2 we provide tentative relations for a transition from the nucleon–nucleon to nucleus–nucleus reactions.

4.1. *The working formulae*

The present approach to the study of the transverse momentum spectra is basically the same as that of WA80 Collaboration.[13] One has to remember in this context that the parametrization that is necessary for producing fits to the data on inclusive cross-sections must accommodate for p_T-dependent variations in the curvature of the spectra. At modestly high transverse momentum values the physics of perturbative QCD is assumed to play and is held by majority to be justified. We pick up here the QCD-inspired parametrization for inclusive cross-section in PP collisions used by WA80 group in an energy-scaled manner; and propose, thereafter, a suggestive form of relationship between inclusive production of pions in hadron–nucleus/nucleus–nucleus collisions and that for PP collision.

The form of the expression to fit the data on inclusive cross-section for pion productions in PP collisions, as proposed by WA80 Collaboration,[13] is given by

$$E\frac{d^3\sigma}{dp^3}(\mathrm{PP})^{\pi^0 X} = \acute{C}\left(\frac{p_0}{p_T + p_0}\right)^n, \tag{9}$$

where $\acute{C}$ is an arbitrary constant, $p_0 = 4.9 \pm 0.3$ and $n = 34 \pm 1$.

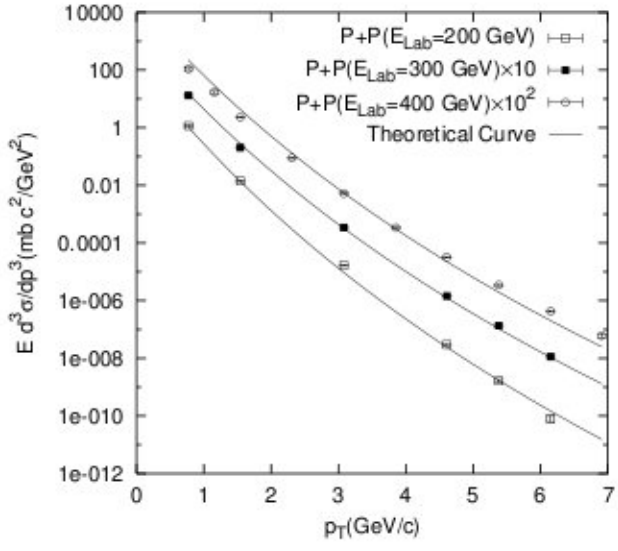

Fig. 11. Plot of $E\frac{d^3\sigma}{dp^3}$ versus p_T for production of secondary pions in PP collisions at $E_{\rm Lab} = 200$, 300 and 400 GeV. The various experimental points are from Ref. 25 and the solid curves are based on Eq. (9).

In so far as PP collision is concerned, the WA80 collaboration tested the above relationship given by Eq. 9, at $E_{\rm Lab} = 200$ GeV. However, in the present work, we have checked the same expression for PP reactions at two other energies also and they are $E_{\rm Lab} = 300$ GeV and $E_{\rm Lab} = 400$ GeV. It is found that the above expression matches with the data on PP reactions at all the three energies quite well (Fig. 11).

Following the WA80 Collaboration[13] the connection that we want to build up would rest on the following observations[14] — related mainly to nuclear enhancement — anomalous or otherwise: (i) strong dependence on both target and projectile mass, (ii) weak or null rapidity dependence, (iii) weak (if any) $\sqrt{s}$ dependence, (iv) impact parameter dependence restricted to collisions without full overlap of target and projectile, (v) strong p_T dependence.

4.2. *The switchover to nuclear collisions: A clue*

On the basis of these observations the proposed form of the fit for inclusive production of pions at high energies in various nucleus(A)–nucleus(B) (Figs. 12–17) interactions is offered by the expression given by Eq. (3):

$$E\frac{d^3\sigma}{dp^3}\bigg|_{(\rm AB)\to\pi^0 X} = ({\rm A}\cdot{\rm B})^{g(p_T)} E\frac{d^3\sigma}{dp^3}\bigg|_{(\rm PP)\to\pi^0 X}, \tag{10}$$

where $g(p_T)$ has been cast in the mould of $g(p_T) = 1 + \lambda p_T$ where λ is the coefficient of p_T. The linear dependence of $g(p_T)$ on p_T is prescribed here in accordance

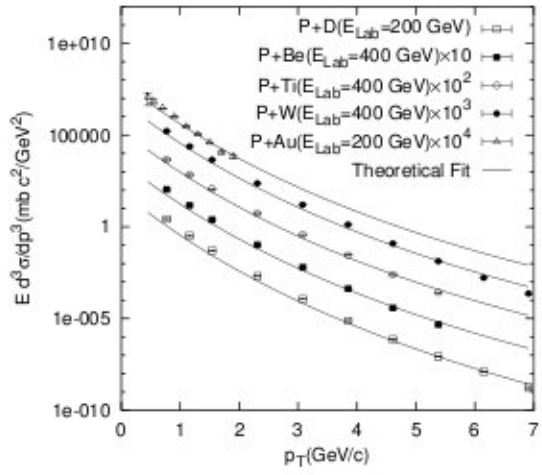

Fig. 12. The inclusive spectra for secondary pions produced in different proton–nucleus collisions at $E_{\mathrm{Lab}} = 200$ and 400 GeV. The various experimental points are from Refs. 17 and 26. The solid curves represent the theoretical fits on the basis of Eq. (10).

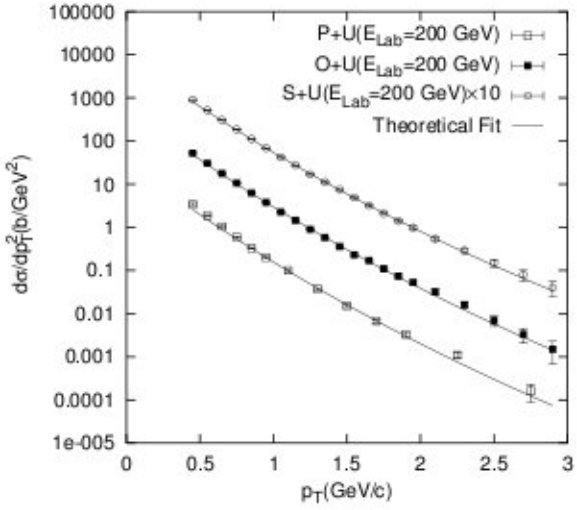

Fig. 13. Plot of $\frac{d\sigma}{dp_T^2}$ for secondary pions in different nucleus–uranium collisions at $E_{\mathrm{Lab}} = 200$ GeV/nucleon as a function of transverse momentum p_T. The various experimental data are taken from Ref. 27. The solid curves represent the theoretical fits on the basis of Eq. (10).

with what is known as the Cronin effect, as the major part of the available data addresses p_T-values only beyond $p_T = 0.8$ GeV/c.[15–17] This effect is valid in the range 0.8 GeV/c $\leq p_T \leq$ 3 GeV/c. The Cronin effect is due to scattering of partons or pions in the target nucleus. This leads to the so-called "anomalous nuclear enhancement" (ANE) of high-p_T hadrons. Unless sufficient and reliable data are available for particle–nucleus and nucleus–nucleus collisions in the range of

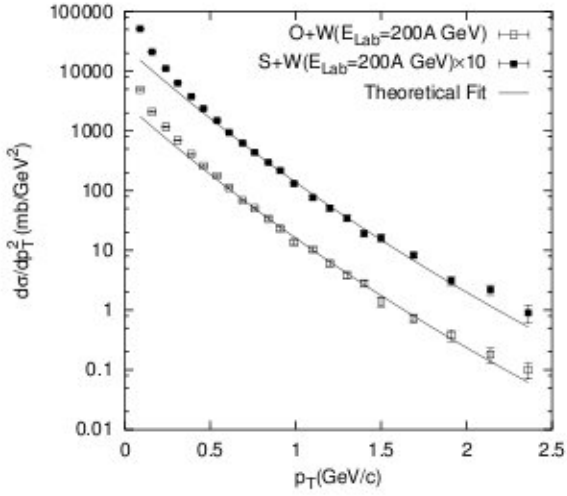

Fig. 14. Nature of $\frac{d\sigma}{dp_T^2}$ for production of secondary pions in O–W and S–W collisions at $E_{\rm Lab}$ = 200 A GeV on transverse momenta. The various experimental points are taken from Ref. 15. The solid curves are drawn on the basis of Eq. (10).

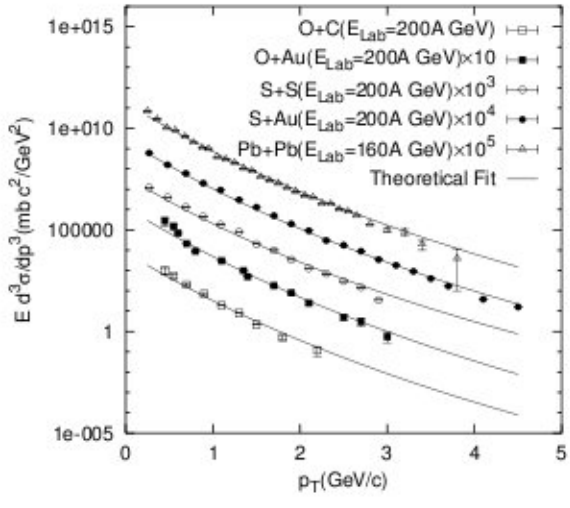

Fig. 15. Nature of inclusive spectra for production in secondary pions in various nucleus–nucleus collisions at two different energies with changes of transverse momenta. The various experimental points are from Refs. 13, 26 and 28. The solid curvilinear lines represent the theoretical fits on the basis of Eq. (10).

$p_T < 0.8$ GeV/c, no definite conclusion on the validity of the expression (10) for the soft-interaction domain could here be made. In addressing the data on meson production in some of the collisions through model-based calculations, we assume that pions overwhelmingly dominate all other non-pion varieties of secondary mesons; and so we have reasonably neglected them for all practical purposes.

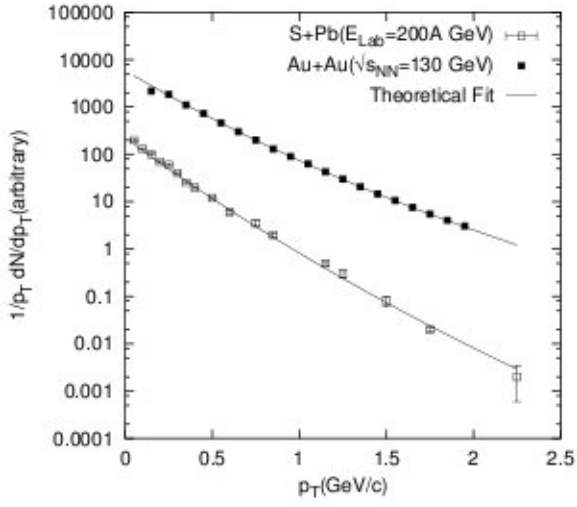

Fig. 16. Invariant spectra for production of secondary pions in S–Pb and Au–Au collisions at $E_{\mathrm{Lab}} = 200$ A and $\sqrt{s_{NN}} = 130$ GeV respectively. The various experimental points are from Refs. 29 and 30. The solid curvilinear lines represent the theoretical fits on the basis of Eq. (10).

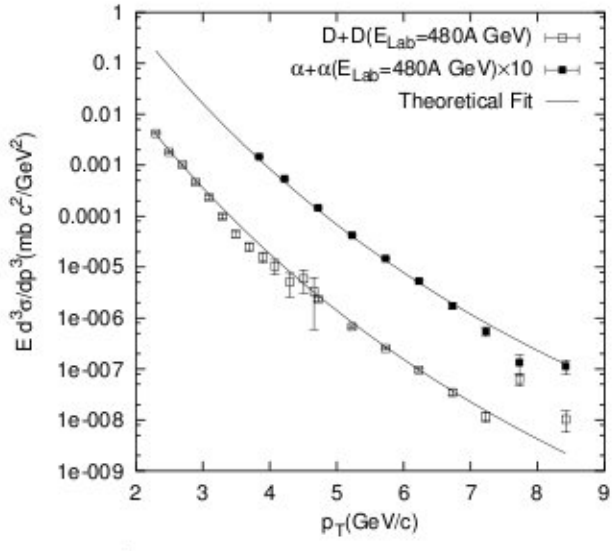

Fig. 17. Dependence of $E\frac{d^3\sigma}{dp^3}$ of secondary pions produced in D–D and $\alpha - \alpha$ collisions at $E_{\mathrm{Lab}} = 480$ A GeV on the values of p_T. The various experimental points are from Refs. 31 and 32. The solid curves represent the theoretical fits on the basis of Eq. (10).

The $(\mathrm{A} \cdot \mathrm{B})$ dependence of λ has been depicted in Fig. 18 and the curve can be phenomenologically expressed by the relation:

$$\lambda = -0.032 + \frac{1.128}{\ln(\mathrm{A} \cdot \mathrm{B})}\,. \tag{11}$$

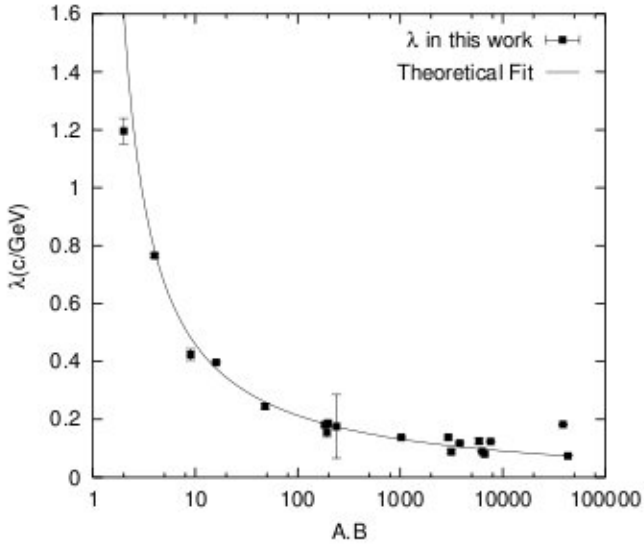

Fig. 18. Values of λ as a function of (A · B). The various data-type points are from Table 3 and the solid curve is drawn on the basis of Eq. (11).

Table 3. The nuclear collisions at different high energies: values of the p_T-coefficient.

Collision	E (GeV)	λ	χ^2/ndf
P + D	200	1.196 ± 0.044	0.240
P + Be	400	0.424 ± 0.020	0.232
P + Ti	400	0.245 ± 0.011	0.189
P + W	400	0.181 ± 0.007	0.206
P + Au	200	0.187 ± 0.009	0.059
P + U	200	0.176 ± 0.11	0.820
D + D	480 A	0.766 ± 0.006	0.011
$\alpha + \alpha$	480 A	0.397 ± 0.003	0.30
O + C	200 A	0.156 ± 0.017	0.459
O + W	200 A	0.138 ± 0.007	0.605
O + Au	200 A	0.088 ± 0.007	0.617
O + U	200 A	0.118 ± 0.004	0.910
S + S	200 A	0.138 ± 0.002	0.326
S + Au	200 A	0.090 ± 0.001	0.002
S + W	200 A	0.125 ± 0.009	1.652
S + Pb	200 A	0.081 ± 0.005	1.674
S + U	200 A	0.124 ± 0.002	0.323
Au + Au (RHIC)	8450 A	$0.183 \pm .001$	1.141
Pb + Pb	160 A	$0.074 \pm .0001$	0.144

The relationship shows that larger is the product-value of (A·B), lower would grow the value of coefficient of p_T and also $g(p_T)$. The linear nature of p_T dependence is now established.

A few comments on the nature of transverse momentum spectra are in order here: (i) The $E\frac{d^3\sigma}{dp^3}$ versus p_T spectra, starting from PP collisions at ISR range of energies to heavy ion collisions, like Pb–Pb collision at $E_{\mathrm{Lab}} = 160\,\mathrm{A}$ GeV at SPS, the RHIC data on Au–Au collision at $\sqrt{s_{\mathrm{NN}}} = 130$ GeV and many other reactions have here been presented in the diagrams (Figs. 11–17). (ii) However, the only exceptions are the P–U, O–U, S–U, O–W, S–W, S–Pb and Au–Au collisions (Figs. 13, 14 and 16) for which $\frac{dN}{dp_T^2}$ or $\frac{d\sigma}{dp_T^2}$ versus p_T (instead of $E\frac{d^3\sigma}{dp^3}$ versus p_T) data was available. The formula for the fit has been necessarily adjusted for the corresponding changes in the observable. (iii) The p_T coefficient term in the exponential term has a logarithmic nature of dependence with the values diminishing for higher range of (AB) product terms. This is consistent with the nature of relationship shown in the expression (11). (iv) In providing the fits in all the diagrams here suitable normalization of inclusive cross-sections has always been done, whenever it is necessary. It is to be noted that we consciously concentrate here on tracing mainly the qualitative nature of the transverse momentum plots and seeking consistency in the quantitative values within the acceptable graphical patterns of the plots.

5. Discussion and Concluding Remarks

By all accounts, both rapidity and transverse momentum spectra of the pion secondaries produced in nucleon–nucleus and nucleus–nucleus collisions show up striking agreement between the calculated results and the measured data. If the measurements are to be relied upon, the findings made here lead to the affirmation, to a considerable degree, of the intrinsic merit and worth of the patterns of expressions which were here put into use. This is, especially, true of the very foundational relation that this work is essentially based on. The suggested forms seem to be quite efficient, as we can obtain satisfactory fits to the data considered over a wide range of energies and for many different interactions by using a small number of phenomenological parameters. The relations and the forms of expressions are also quite simple in nature and this simplicity is its strength as well.

Some further comments are in order here. The fits, almost unexceptionably, look better and more attractive for high to higher energies and for values of the intermediate range of p_T or y values. In so far as the transverse momentum dependence is concerned, this is natural because (i) it is well known that the accuracies of measurements in experiments suffer for both very low and very large values (theoretically this could be ascribed to the nonperturbative effects or extremely-perturbative consequences respectively); (ii) for the larger values of transverse momentum some new physical effects might come into play. For example, the predictions of the constituent interchange mechanism (CIM) and the complications arising thereof might

have played some role to disturb/distort the fits. In case of the rapidity spectrum as well, the first factor is certainly operational but, to our knowledge, we fail to attribute any similar second factor for it. It is to be noted that the quality of fit is somewhat uniform for all studied nucleus-involved reaction(s) from $A = 2$ to $A = 238$ with appropriate focus on $A = 207$. In our opinion, this is an important and physically significant observation.

There are a few specific diagrams here which necessitate and warrant our special attention. In both the diagrams of Fig. 3 we observe that at asymptotic energies there is either no rise or slow rise of C and y_0 values with increase in energy-values. These saturations, in reality, lead essentially to an indication of the very neighborly values of the $\frac{dN}{dy}$ $\left(\text{or } \frac{dN}{d\eta}\right)$ values versus y (or η), as the case may be. This is roughly borne out by experiments as well. In understanding the nature of Fig. 18, one has to simultaneously look at this diagram, the expression in Eq. (11) and Table 3; and then try to analyze carefully. In order to avoid complications we assume, at least initially and for the present, the validity of Feynman scaling through energy-independence, and thus accept only the p_T-dependence. The nature of dependence of this differential (inclusive) cross-section on mass numbers of the projectile and the target is manifested through the values of $g(p_T)$ which has a clear linearized relationship with scaled p_T; and the coefficient of p_T terms depicts an inverse logarithmic behavior on the product of the mass-numbers, A and B. In the Fig. 18 the value of the exponent parameter in the latest RHIC experiment at BNL seems to be the only exception in failing to conform to the general behavior exhibited by all other reactions at various energies. This is probably only natural, because the interaction energy in Au–Au collision at RHIC is too high in comparison to the measurements done in all other nuclear reactions. However, on an overall basis, the diagram (Fig. 18) provides a natural description of its physical nature with highest value of it for low AB and smaller value for the larger ones. This is also captured by the physical behavior reflected in the diagrams (Figs. 12–17). Or, in the other words, the nature shown by the diagram of Fig. 18 is the consequence of the individual behavior exhibited in all of these diagrams.

Lastly, let us, once more, reiterate the gross limitation of the present work. The parameter values that are inducted for obtaining the remarkably good fits in the numerous figures could right now not be given any physical basis and meaning. Indeed, the case is probably no better with all other existing models which suffer from the same or similar problem. But, the fact is so far, they did not achieve or report such a wide and extensive experimental support as is demonstrated here; nor do they possess such a structural uniformity of pattern in both the basic working formula and in the final useable relations as is envisaged and evidenced here. This fact alone gives the set of models used in the present work an edge over them. In the near future we will try to deal with this useful and economical approach the other varieties of secondaries, like kaon–antikaons, baryon–antibaryons, etc. Besides, further refining the basis of the p_T-spectra obtained here is also very much on the agenda of our work with the top most priority.

Acknowledgments

It is a pleasure to thank heartily the honourable anonymous referee for his valuable suggestions on compactification of an earlier version of this manuscript and also Professor Michael Spalinski, one of the editors of IJMP(A), for his all-time kind and prompt correspondences with us.

Besides, the authors would like to acknowledge the stimulus received from the honourable referee of one of our previously published paper in European Physical Journal A. Furthermore, we are also indebted to Professor Peter Seyboth and Professor Thomas Peitzmann of various collaborations for some very helpful correspondences and/or comments.

One of the authors, PGR, is grateful to the UGC (India) for its financial support through the Faculty Development Programme.

Noted Added in Proofs

There was an oversight and thus an omission on our part to mention the fact that the fits of a similar form as those of Eqs. (5) and (6), of course, with the different parameter-values, were suggested by Wong[23] long before. This was detected by ourselves only very recently. Though we proceeded independently and this parametrization is not the main focus of the present work, the oversight is sincerely regretted.

References

1. B. De and S. Bhattacharyya, *Eur. Phys. J.* **A10**, 387 (2001).
2. S. Bhattacharyya and B. De, *Mod. Phys. Lett.* **A21**, 1395 (2001).
3. T. Peitzmann, *Phys. Lett.* **B450**, 7 (1999).
4. H. R. Schmidt and J. Schukraft, *J. Phys.* **G19**, 1705 (1993).
5. W. Thome' *et al.*, *Nucl. Phys.* **B129**, 365 (1977).
6. G. J. Alner *et al.* (UA5 Collaboration), *Phys. Rep.* **154**, 247 (1987).
7. F. Demarteau *et al.*, Fermilab-Conf-92/103 April 1992.
8. S. Bhattacharyya, *Lett. Nuovo Cimento* **44**, 119 (1985).
9. R. C. Hwa *et al.*, *Phys. Rev.* **C64**, 054611 (2001).
10. *Introduction to High-Energy Heavy-Ion Collisions*, C. Y. Wong (World Scientific, Singapore, 1994).
11. The Axial Field Spectrometer Collaboration, *Phys. Lett.* **B108**, 58 (1982).
12. M. M. Aggarwal and S. I. A. Garpman, *Int. J. Mod. Phys.* **E4**, 477 (1995).
13. R. Albrecht *et al.* (WA80 Collaboration), *Eur. Phys. J.* **C5**, 255 (1998).
14. J. Schukraft, CERN-PPE/91-04, 16 January, 1991.
15. T. Akesson *et al.*, *Z. Phys.* **C46**, 361 (1990).
16. J. W. Cronin *et al.*, *Phys. Rev.* **D11**, 3105 (1975).
17. D. Antreasyan *et al.*, *Phys. Rev.* **D19**, 764 (1979).
18. J. Geiss *et al.*, *Nucl. Phys.* **A644**, 107 (1998).
19. T. Abbott *et al.* (E-802 Collaboration), *Phys. Rev.* **C50**, 1024 (1994).
20. Alber *et al.*, http://durpdg.dur.ac.uk/cgi-bin/hepdata/testreac/9338/FULL/q.
21. J. Barrette *et al.* (E877 Group), *Nucl. Phys.* **A610**, 153c (1996); *Phys. Rev.* **C62**, 024901 (2000).

22. J. Bachler *et al.*, *Nucl. Phys.* **A661**, 45c (1999).
23. C. Y. Wong, *Phys. Rev.* **D30**, 961 (1984).
24. B. B. Back *et al.* (PHOBOS Collaboration), *Phys. Rev. Lett.* **87**, 102303 (2001).
25. D. Antreasyan *et al.*, *Phys. Rev. Letts.* **38**, 112 (1977).
26. WA80 Collaboration, *Z. Phys.* **C38**, 97 (1988).
27. M. C. Abreu *et al.* (NA38 Collaboration), *Z. Phys.* **C55**, 365 (1993).
28. T. Peitzmann: http://alice.web.cern.ch/Alice/qm97/peitzmann/index.html.
29. Z. Wlodarczyk, Proc. of the xxiii ICRC, Invited, Rapporteur & Highlight Papers (Calgary, Alberta, Canada 19–30 July 1993), eds. Leahy Hicks and Venkatesan (World Scientific, Singapore, 1994), p. 355.
30. C. Adler *et al.* (STAR Collaboration), *Phys. Rev. Lett.* **87**, 112303 (2001).
31. A. L. S. Angelis *et al.* (BCMOR Collaboration), *Phys. Lett.* **B185**, 213 (1987).
32. A. G. Clark *et al.*, *Nucl. Phys.* **B142**, 189 (1978).